An integrated SCAL study for estimating wettability and relative permeability

Raheleh Farokhpoor [1] *, *Andrew Fogden* [2], *Egil Boye Petersen* [1]

[1] AkerBP, Norway, [2] Wintershall DEA, Germany

Abstract. In an appraisal phase of the life cycle of an oil and gas project, timing and costs are important when gathering information for assessing economic viability of the project. Reservoir rock and flow properties play a crucial role for estimating the hydrocarbon in-place and recoverable. Despite establishing a laboratory SCAL study in an early phase, it often takes 1-2 years to acquire wettability and relative permeability curves as input to the reservoir models.

In the current work, we present different technologies to first test multiple approaches for determining the wettability and relative permeability and second to accelerate the process and reduce the cost and uncertainty of such data. The work started with measuring steady-state relative permeability curves using a standard core flooding experiment. The results were somewhat unexpected and raised questions regarding core preparation. Therefore, a suitable cleaning method was then examined, in which four sister core plugs were cleaned with so-called mild to harsh approaches and changes in rock properties and wettability were measured.

Preserved core materials were then selected from various facies of the reservoir in the oil zone. 1.5-inch core plugs were cleaned by the selected method and petrophysical properties were measured. The core plugs were then restored with crude oil at reservoir temperature. Their wettability was characterised by two methods, NMR and Amott-USBM. There was a good consistency in wettability results from NMR and centrifuge, showing that NMR wettability index can be an efficient and cheaper means to estimate wettability.

After the SCAL study, the core plugs were 3D imaged with micro-CT, from which the main small-scale rock-types were subsampled for high-resolution imaging. After image processing for pore segmentation, pore-scale flow simulations were performed on each subsample. Pore-scale wettability descriptors were tuned to match the resulting capillary pressure curves to the corresponding lab Amott-USBM, from which relative permeability curves were compared to the lab and data-based results.

An analytical approach for determining relative permeability was also employed in this work. First, petrophysical properties were used to find suitable analogue data, from which wettability and endpoint saturation and endpoint relative permeability data were applied to validate the trapping model and tune the shape of the relative permeability curves.

1. Introduction

In an early phase of a field development plan, dynamic reservoir properties such as relative permeability curves are essential to initialize a reservoir model. Uncertainties in relative permeability and trapping phase model often lead to large uncertainties in estimating the reserves.

During the field production phase, history matching is used to tune relative permeability curves in the model, which are called pseudo relative permeability curves. These curves take into account heterogeneity and represent a large section of the reservoir, which can be very different from relative permeability curves measured in the SCAL laboratory on core samples.

In this paper, a range of core flooding experiments on preserved core materials from a section of reservoir with similar facies are presented. The experiments include steady-state relative permeability, wettability, single speed and multi speed centrifuge and porous plate tests. The experiments were performed in three different laboratories, due to availability and capacity. It is worth mentioning that the whole program was not planned from the beginning, but rather evolved from the need to explain unexpected results.

As it was not possible to achieve reliable relative permeability curves from the contradictory experimental results, other methodologies were introduced, namely digital rock and analytical methods. Wettability determined by laboratory SCAL is an important input for digital rock to correctly simulate relative permeability.

The final step in estimating relative permeability was an analytical approach, combining all existing experimental data with analogue data. A trend model for LET parameters and endpoint saturation and relative permeability is tuned to the experimental and best analogue data [1], [2].

2. Lithology of core material

Core materials were taken with water-based mud from an upper Synrift formation from a discovery well in the Norwegian North Sea. Whole core sections (10 cm in diameter and 20 cm long) were cut from the cores and wrapped in cling film and aluminium foil, then preserved in Ergoseal plastic impermeable coating for long term storage.

* Corresponding author: raheleh.farokhpoor@akerbp.com

From a sedimentological depositional environment, the samples are characterized mainly as sandy alluvial plain, with average porosity values between 12-17% and permeability ranging from 10 to 200 mD. The texture of most plugs is classified as a poorly to very-poorly sorted medium-grained (250-500 µm) sand, which is distinctly laminated due to variation in grain size. Common to abundant quartz and feldspar grains are covered by very thin, tangential illite rims. Pores are up to 200 µm in size, and intergranular porosity is moderate with sparse intragranular and moldic pores due to (partial) dissolution of feldspar grains. Reservoir quality is moderate due to carbonate cement which reduced porosity and pore connectivity. **Fig. *1*** shows a thin section under plain polarized light from a core material at 40 times magnification (500 µm resolution).

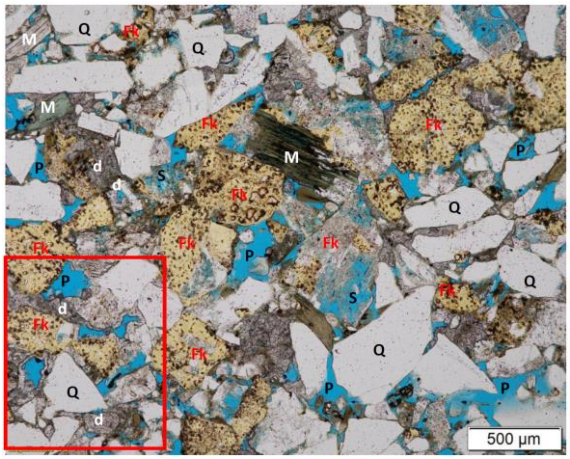

Fig. 1. Porosity (blue), Q: quartz, Fk: K-feldspar, M: mica, d: dolomite cement. Intergranular (P) and intragranular (S) pores are visible. In red box, common pore-filling dolomite (d) is the main authigenic cement in this sample.

3. Experimental analysis

Various experimental analyses were performed on preserved core materials from comparable formations and facies. The first round of experiments comprised steady-state water/oil core flooding on four samples, performed in Lab-1. For simplicity, only the result for the best sample is reported in this paper. Most plugs showed strong capillary end effect and a marked water-wet behaviour with a very small flow window, which raised questions regarding the cleaning process and wettability restoration.

Therefore, a second round of experiments performed in Lab-2 were designed to define a suitable cleaning approach. Different cleaning methods were applied to sister core plugs, after which petrophysical properties and wettability determination by Amott testing were used to characterize the cleaning methods. A preferred method was thus selected to clean core plugs for further SCAL analysis.

The third round of experiments in Lab-3 used new preserved core material from a similar formation, on which petrophysical properties, endpoint saturation and endpoint relative permeability were measured. Wettability of the core plugs was determined by two methods: NMR and Amott-USBM test [3] [4]. Details of the experimental analysis and main results are presented in the following three sections.

Core plugs from Lab-3 were then sent to the digital rock laboratory for analysis down to micro-scale. Core plugs and sub-plugs were 3D imaged with micro-CT at low- and high-resolution, respectively. To capture sub-resolution pores, SEM 2D imaging with EDS mineral mapping was employed. The details of imaging processes and pore network modelling and flow properties simulation are given in the digital core analysis section.

3.1 Steady-state relative permeability experiments (Lab-1)

Steady-state water/oil core floods were performed on restored-state composite cores at semi-reservoir conditions: 80° C, 10 bar pore pressure and net confining stress of 143 bar. The plugs were cleaned by flooding of ca. 100 ml of synthetic formation water (SFW) and then alternating sequences of methanol, a 50/50% mix of methanol and toluene, followed by toluene, in a continuous loop at 60 °C with back pressure of ca. 3 bar.

The cores were saturated with SFW by miscible displacement until stable impedance over each core was obtained. They were then drained to initial water saturation (S_{wi}) using stock tank oil (STO), which aimed to simultaneously restore reservoir wettability after 4 weeks of maintaining the cores at 80 °C and pore pressure of 7 bar.

The SFW has a density of 1035 kg/m^3 and viscosity of 1.26 cP at standard conditions. The reservoir oil is light with STO density of 860 kg/m^3 and viscosity of 4.4 cP at standard conditions. **Table 1** presents the key parameters of the core plugs. Water/oil steady-state relative permeabilities for the composite core are visualised in **Fig. *2***.

Table 1. Core plug properties for the flooding experiment (Lab-1).

Core plug	Helium Porosity	Klink. Permea-bility	K_w (S_w=1)	S_{wi}	K_O (S_{wi})
	(frac.)	(mD)	(mD)	(frac.)	(mD)
Plug 1	0.144	114	64.2		79.5
Plug 2	0.140	104	62.2		100
Composite	0.138		28.8	0.18	71.1

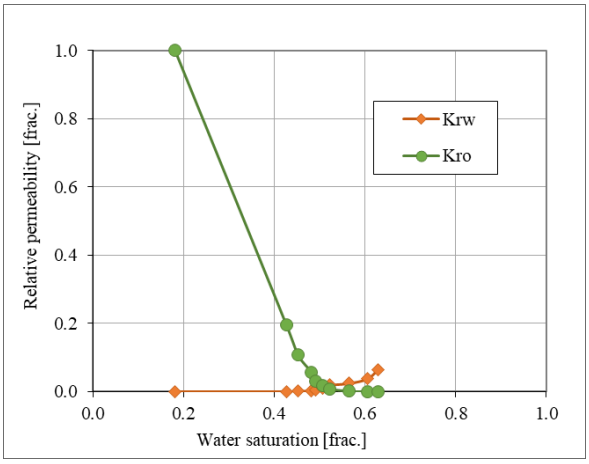

Fig. 2. Water/oil steady-state relative permeability curves (Lab-1).

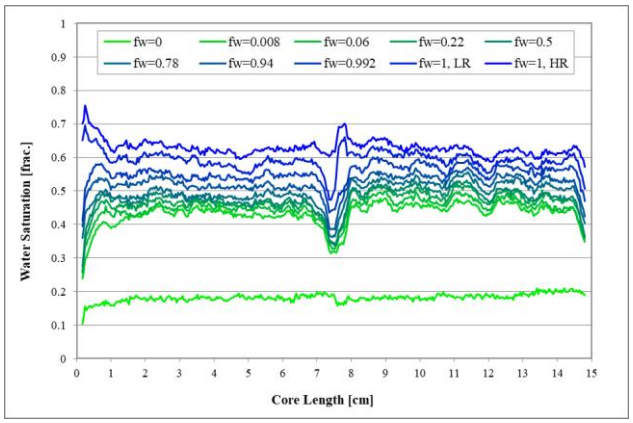

Fig. 3. Saturation profile along composite plug (Lab-1).

In order to increase X-ray attenuation of the water phase, iodide doped SFW was used to capture the saturation profile with ISSM. The water saturation profiles for the progression of flow fractions are plotted in **Fig. 3**.

The flat saturation profiles show negligible capillary end effect, partly due to history matching of the production to refine the measured data. After the bump flow (High Rate HR), residual oil saturation (S_{or}) is 0.370 (frac.) and water relative permeability K_{rw} (S_{or}) is 0.065. Such high saturation and very low K_{rw} of the endpoint did not seem reasonable, as it suggests a strongly water-wet state. Therefore, wettability of the two sister core plugs from the steady-state floods was measured by Amott-USBM testing, as listed in **Table 2**. These experiments show that the plugs are neutral- to water-wet, which contradicts the strong water-wet scenario.

Table 2. Wettability by Amott-USBM test (Lab-1).

Index	Core 1	Core 2
Amott-Harvey	0.22	0.19
USBM	0.24	0.42
Wettability	neutral to water wet	

Accordingly, further studies were performed to investigate the effect of cleaning on wettability and to decide on the best method. Endpoint flow properties were subsequently measured on restored core plugs and used to simulate relative permeability curves.

3.2 Comparison of cleaning methods (Lab-2)

The main objective of the Lab-2 study was to characterise how wettability and permeability may be altered by exposing the cores to different cleaning methods. In total, 8 core plugs were drilled from a preserved core section (Seal Peel #14, **Fig. *3***). Four different cleaning procedures were applied to the cores. For each such method, two parallel experiments were performed on twin core plugs taken from the same depth of the preserved core to check reproducibility. The procedure was as follows:

1. All core plugs underwent mild cleaning (mild cleaning 1) by alternating flooding with mineral oil (Isopar L) and SFW at 70 °C and a volume rate of about 60 ml/hr for several weeks.
2. 2 core plugs (twin plugs 1A and 1B) were run in a centrifuge directly after mild cleaning 1 to establish S_{wi}, after which oil permeability at S_{wi} was measured, prior to Amott testing.
3. After mild cleaning 1, two core plugs (twins 2A and 2B) were further cleaned by flooding at room temperature by injection of sequences of Isopar L, methanol and SFW (mild cleaning 2). Absolute permeability to oil, methanol and water was measured after each flooding. The plugs were then centrifuged to establish S_{wi}, followed by measurement of K_o (S_{wi}) and then Amott testing.
4. After mild cleaning 2, the remaining 4 plugs underwent further cleaning in a Soxhlet apparatus: 2 plugs (twins 3A and 3B) were extracted in toluene (cleaning 3) and the other 2 plugs (twins 4A and 4B) were extracted in dichloromethane (DCM)/methanol mixture (cleaning 4). After Soxhlet cleaning, core plugs were flooded with Isopar L, methanol and SFW, followed by permeability measurement after each flooding. They were then centrifuged at 10 000 rpm to establish S_{wi}. Oil permeability at S_{wi} was measured on these plugs before starting the wetting tests.
5. Finally, after wettability testing, the cores were Soxhlet cleaned in methanol and then in toluene for 10-12 days until no discolouration of solvents was observed. Afterwards, these plugs were dried in an oven at 60 °C to prepare for porosity and permeability measurements.

Fig. 4. Core plugs drilled from preserved core #14 (Lab-2).

Table 3. Oil permeability after each cleaning method (Lab-2).

Plug	Clean 1	Clean 2	Clean 3	Clean 4	After Amott	
ID	K oil 2phase	K_{abs} oil	K_{abs} oil	K_{abs} oil	Ko (S_{wi})	KL
	(mD)	(mD)	(mD)	(mD)	(mD)	(mD)
1A	11.7	-	-	-	64.0	108.4
1B	8.7	-	-	-	37.0	47.6
2A	10.1	27.3	-	-	46.1	56.9
2B	10.0	15.9	-	-	26.4	30.3
3A	19.8	68.4	246	-	279.9	212.5
3B	10.6	31.6	212	-	257.7	189.7
4A	28.9	52.8	-	279	305.5	273.3
4B	21.2	51.1	-	299	337.2	291.3

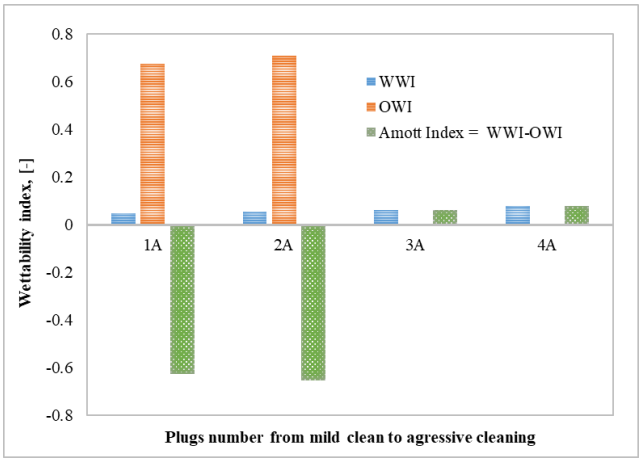

Fig. 5. Amott indexes of core plugs for different cleaning (Lab-2).

Based on the findings in **Table *1*** and **Fig. *3*** from this study of 8 core plugs from the same seal peel, the following conclusions may be drawn:

1. Core properties depend strongly on cleaning procedure.
2. Core permeability increased significantly (by a factor 2-3) after strong cleaning (Soxhlet with harsh solvents), compared to mild cleaning.
3. Wettability was altered from oil-wet condition after mild cleaning (Amott-Harvey index ca. -0.6) to weakly water-wet (Amott Harvey index ca. 0.06) after harsh cleaning. No spontaneous imbibition of oil was observed after harsh cleaning, while spontaneous imbibition of water and especially oil was observed after mild cleaning.
4. Harsh cleaning extracted heavy oil components from the core which remained in the core after only mild cleaning. Cleaning appears to extract components from the core which are not present in the STO (from GC and FT-ICR of effluents/solvents), containing S, N and O. Restoration of wettability by aging in STO or live oil may therefore not be feasible.
5. Interpretation of FT-ICR analysis also indicated larger amounts of medium heavy components in extracts from harsh cleaning. This suggests that some components which are adsorbed to the rock may not be very heavy.
6. No difference was observed between toluene and DCM with 7% methanol in Soxhlet cleaning. However, toluene gave a clear solvent in a shorter time, implying a faster cleaning process.

3.3 Comparison of wettability methods (Lab-3)

One preserved core section (10 cm diameter and 20 cm length) from an oil zone was selected for this study. The 38 mm diameter core plug samples were drilled parallel to apparent bedding with SFW. This preserved section was also subsampled for petrographic analysis (thin section, SEM and XRD whole rock and clay fraction) and high-pressure mercury injection (MICP) on cleaned and dried samples.

The core plugs were cleaned by Cleaning Method 4 from Section 3.2, using the DCM/methanol mixture. Petrophysical properties were then measured, following which one plug was chosen for wettability analysis using NMR wettability index [5] and Amott-USBM method.

The cleaned and dried plugs were first fully saturated with SFW, then spun by centrifuge to the target S_{wi} by injection of STO. The samples were then aged in STO at reservoir conditions (80° C and 190 bar) for 4 weeks. Afterwards, the STO in the plugs was replaced first by decalin (as intermediate solvent) and then by Soltrol oil. The plugs were then transferred to Amott cells filled with SFW for monitoring of brine spontaneous imbibition, before being loaded into the centrifuge for forced imbibition. After establishment of Sor, the Amott test and centrifuge procedure was repeated for oil secondary drainage. Capillary pressure curves are plotted versus water saturation in **Fig. *6***. Based on this data, two types of wettability indices are calculated, the USBM wettability index and Amott-Harvey index.

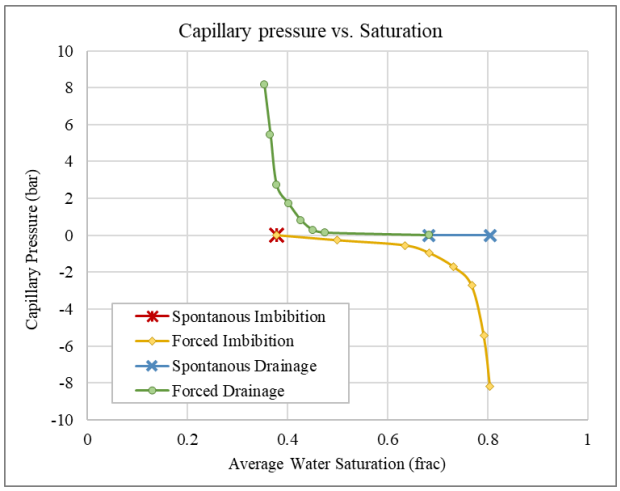

Fig. 6. Capillary pressure vs. saturation from combined Amott-USBM experiment (Lab-3).

NMR response varies as a function of wettability change in core plugs. The NMR T_2 spectra of bulk oil, bulk brine and core plug at $S_w = 1.0$ (frac.) and the core plug at S_{wi} after aging with STO are used to develop an NMR wettability index (NWI). T_2 relation time is plotted in **Fig. *7*** for a core plug at $S_w = 1.0$ (frac.) and for the same plug after flooding with STO at $S_{wi} = 0.380$ (frac.) and aging for 4 weeks. The shift in T_2 peak is attributed to the core wettability alteration.

Wettability index of the core plug thus inferred from Amott-Harvey, USBM and NMR is listed in **Table *4***. All three methods are in very good agreement and predict a wettability state of neutral- to weakly oil-wet.

Table 4. Wettability estimation from combined Amott-USBM and NMR methods (Lab-3).

S_{wi} (frac.)	NWI	Amott-Harvey Index	USBM Index	Wettability
0.380	-0.31	-0.27	-0.20	Neutral to weakly oil-wet

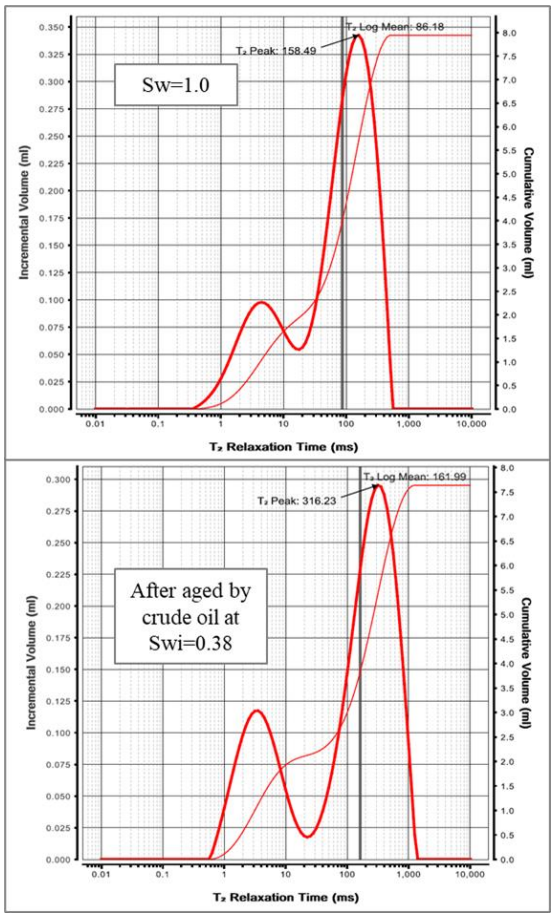

Fig. 7. T_2 relaxation time for core plug at top) 100% water saturation and at bottom) S_{wi} after aging (Lab-3).

4. Digital core analysis

The sister SCAL plug to that used in Section 3.3 was the subject of digital core analysis. The workflow for sampling, imaging and processing comprised the following steps:

1. Micro-CT 3D low-resolution imaging (non-destructive) of the plug in cleaned dried state, for subsample selection and upscaling. Cutting of a 2 cm thick trim-end on which all work was performed.
2. Saturation of trim-end using SFW doped with 1 M sodium iodide (NaI), for weighing and micro-CT 3D low-resolution imaging.
3. Primary drainage (PD) of trim-end by single-speed centrifugation in air in both directions (capillary pressure Pc = 2.5 bar oil-water equivalent), for weighing and micro-CT 3D low-resolution imaging.
4. Cleaning of trim-end by immersion in methanol at 50 °C and subsampling using high-precision diamond saw for micro-CT 3D high-resolution imaging and SEM 2D mapping with back-scattered electrons (BSE) and energy-dispersive X-ray spectroscopy (EDS) for automated spatial mineralogy.
5. Processing and segmentation of micro-CT 3D high-resolution images of subsamples (PerGeos software) for pore-scale simulations (eCore software).

Fig. 8 summarizes the imaging performed in steps 1 and 4, starting with the micro-CT 3D low-resolution image in **Fig. *8***a. This plug is faintly laminated parallel to the cylinder axis. Two small-scale rock types could be visually distinguished – one with larger grains and pores (SP_1) relative to the other (SP_2). Steps 2 and 3, combined with image alignment and analysis, yield 3D maps of total porosity φ and PD-endpoint water saturation S_{wi} over the trim-end.

The micro-CT 3D high-resolution images of the two corresponding sub-plugs SP_1 and SP_2 are displayed in ***Fig. 8b*** and ***8c.*** The SEM mineral map over the section perpendicular to bedding is given in **Fig. *9***, along with the modal mineralogy. SP_1 contains larger inter-granular and moldic dissolution pores; however, it also contains more carbonate cement. SP_2 contains finer grains and lithic fragments, including additional detrital illite.

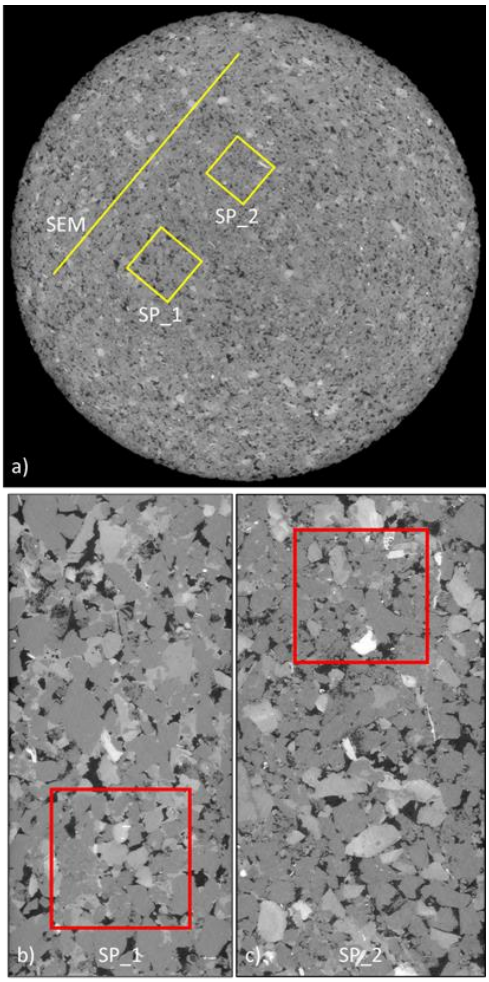

Fig. 8. a) Central cross-sectional slice of micro-CT 3D image of trim-end of plug (width 38.1 mm, voxel 17.1 µm), showing size and targeted small-scale rock types of horizontal sub-plugs SP_1 and SP_2 and orientation of SEM section; central longitudinal slice of micro-CT 3D image of b) SP_1 (width 4.2 mm, voxel 1.65 µm) and c) SP_2 (width 3.8 mm, voxel 1.43 µm), showing size of simulation cubes.

The micro-CT 3D high-resolution images of SP_1 and SP_2 were binary segmented into resolved pore space. Cubes were then cropped from the segmented image for the simulations of petrophysical and dynamic flow properties parallel to bedding. Absolute permeability was simulated using a Lattice-Boltzmann algorithm, with the results shown in **Table 5.** The simulations agree well with lab-measured plug porosity and Klinkenberg permeability.

Table 5. Experimental and simulated petrophysical properties.

Method	Sample	Porosity (frac.)	Permeability (mD)
Experiment	21A	0.165	57.1
Digital core	Sub plug 1	0.168	98.7
	Sub plug 2	0.167	93.9

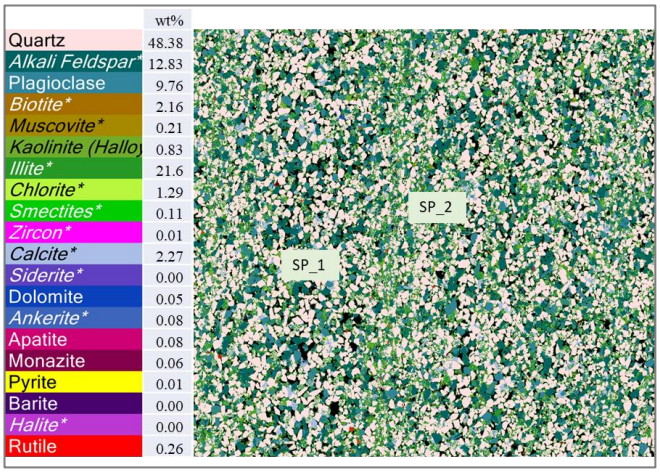

Fig. 9. Overview SEM-EDS 2D mineral map of section (width 23.6 mm, pixel 15 µm), showing mineral colour legend and wt%, and targeted small-scale rock types of SP_1 and SP_2.

The voxelized binary image was also used to simulate by a capillary drainage algorithm the Pc (S_w) curve for PD of brine by oil, using the reservoir density values for these two fluids and an assumed interfacial tension value. The simulation output was post-corrected to add a contribution from pore throats below the micro-CT resolution limit, using pore-size analysis of the corresponding SEM-BSE 2D maps.

The oil-brine relative permeability for PD and subsequent waterflooding (WF) of SP_1 and SP_2 was then pore-scale simulated. At the PD endpoint, wettability alteration is imposed (to mimic the STO aging in Section 3.3) by selection of a set of pore-scale parameters to define the wettability state for subsequent WF. These parameters are the oil-wet pore fraction (variable), the water-advancing contact angle range over unaltered surfaces (fixed at 40-60°) and altered surfaces (110°-variable maximum). These parameters are not physically measured, but rather tuned within established realistic ranges to match the wettability of the core measured in the lab. The wettability parameters for four such cases, called WF-1 to -4, are listed in **Table *6***.

Table 6. Wettability scenarios and resulting endpoints for water flooding simulation on subsamples.

Sub-plug	Wettability	Contact angle	Waterflooding		Amott-Harvey index
Nr#	State #	(deg.)	S_{or} (frac.)	K_{rw} (S_{or})	
SP_1	WF-1	140	0.28	0.21	-0.42
SP_1	WF-2	145	0.25	0.29	-0.35
SP_1	WF-3	150	0.16	0.46	-0.32
SP_1	WF-4	155	0.15	0.54	-0.48
SP_2	WF-1	140	0.25	0.45	-0.26
SP_2	WF-2	145	0.21	0.53	-0.16
SP_2	WF-3	150	0.20	0.60	-0.23
SP_2	WF-4	155	0.17	0.67	-0.21

The increasingly oil-wet conditions from WF-1 to WF-4 increasingly favour meniscus flow, with decreasing residual oil saturation S_{or} and increasing K_{rw} (S_{or}), as expected. Further, S_{or} is typically larger and K_{rw} (S_{or}) is substantially smaller for SP_1, due to its high aspect ratio of large pore bodies to calcite-cement constricted throats.

The low-resolution micro-CT scan shows that distribution of SP_1 and SP_2 are nearly 50:50. Therefore, upscaling from subsamples to plug scale was performed by averaging properties of the two subsamples at fixed capillary pressure. The resulting S_{or} and K_{rw} (S_{or}) and Amott-Harvey index are given in **Table 7**. The upscaled simulated relative permeability curves of water and oil for waterflooding under these 4 assumed wettability states is plotted in **Fig. 10**.

Table 7. Wettability scenarios and resulting endpoints for upscaled simulation of water flooding.

Wettability	Contact angle	Waterflooding		Amott-Harvey index
State #	max (deg.)	S_{or} (frac.)	$K_{rw}(S_{or})$	
WF-1	140	0.27	0.31	-0.34
WF-2	145	0.23	0.39	-0.27
WF-3	150	0.18	0.53	-0.26
WF-4	155	0.17	0.59	-0.33

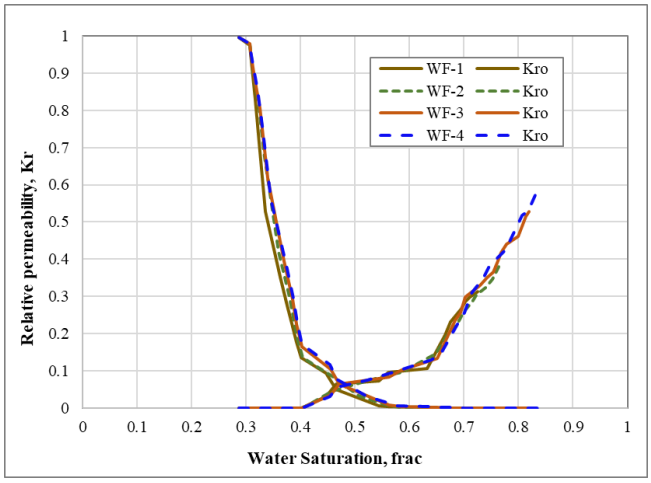

Fig. 10. Simulated water/oil imbibition relative permeability curves of subsamples SP_1 and SP_2 for four wettability scenarios.

An indication as to which pore-scale wettability scenario best matches the lab-restored state can be obtained from comparison to measured endpoint values (from ultra-centrifuge forced imbibition or unsteady-state WF) or Amott-Harvey index. In **Table 6** and **Table 7**, a cut-off of ±0.005 bar was used to define spontaneous imbibition and secondary drainage, to provide more realistic comparison to experiments.

5. Relative permeability modelling with uncertainty using high-quality experiment and analogue data

This study presents a comprehensive approach to obtaining reliable relative permeability curves suitable for reservoir simulation. The methodology combines existing experimental data with high-quality analogue data from a

corporate rock and fluid database [1]. The steady-state imbibition experiments in Section 3.1, including production and differential pressure profiles, are history matched, showing reasonable agreement. The resulting parameterized LET relative permeabilities align well with analytically determined relative permeabilities, as shown in **Fig. *11***. Out of the total of four steady-state experiments mentioned in Section 3.1, only one qualifies as average to high quality and is included in the SCAL model.

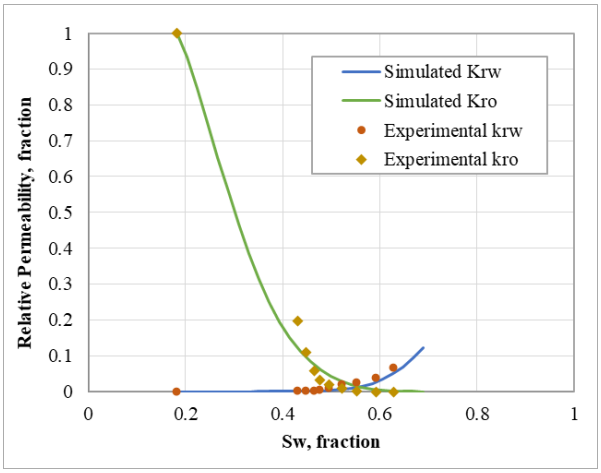

Fig. 11. Simulated and experimental relative permeability curves**.**

In addition, suitable analogue data are used to reduce the model's uncertainty and validate the field experimental data. By generating a new relative permeability curve primarily based on analogues and experimental data, the model is further strengthened [5]. The curve incorporates residual oil saturation and endpoint permeability to water at residual oil saturation, supported by experimental and analogue data. Comparing the resulting relative permeability model with experimental data confirms its accuracy. **Fig. *12*** illustrates the excellent match between our field data (represented in red) and the analogue data for residual oil as a function of initial water saturation. The figure includes experimental data from multi- and single-speed centrifuge, porous plate, steady-state and unsteady-state methods. The highlighted red data from our field agrees well with the analogues for both K_{rw} (S_{orw}) and S_{orw}, except for the steady-state experiments. Some analogue K_{rw} (S_{orw}) vs. S_{wi} data fall outside the uncertainty defined by the model, but the model prioritizes the experimental scenarios that provide the highest accuracy for K_{rw} at S_{wi} measurements. Therefore, these data have not been trusted or used as part of our field SCAL model.

The resulting relative permeability model, along with its uncertainty band, is compared with both experimental data and digital rock data in **Fig. *13***. In the top part of **Fig. *13***, the trend model has been tuned to capture the best analogue data for our field, and the base case has been adjusted to match the best analogue. It can be observed that the relative permeability to oil for our field (indicated in red) falls within the uncertainty band, leaning toward the optimistic side of the relative permeability model. However, the water permeability falls outside the uncertainty band and can be considered an extreme case that should not be trusted.

In the lower part of **Fig. *13***, the relative permeability generated from digital rock is compared with our SCAL model tuned to the rock properties of the digital rock. The data partially reproduce the K_{rw} and K_{ro} in certain saturation ranges but fall outside the model's accuracy at intermediate saturation range. Since the model represents experimental data from both our field and analogues, which likely cover a wider range of rock properties.

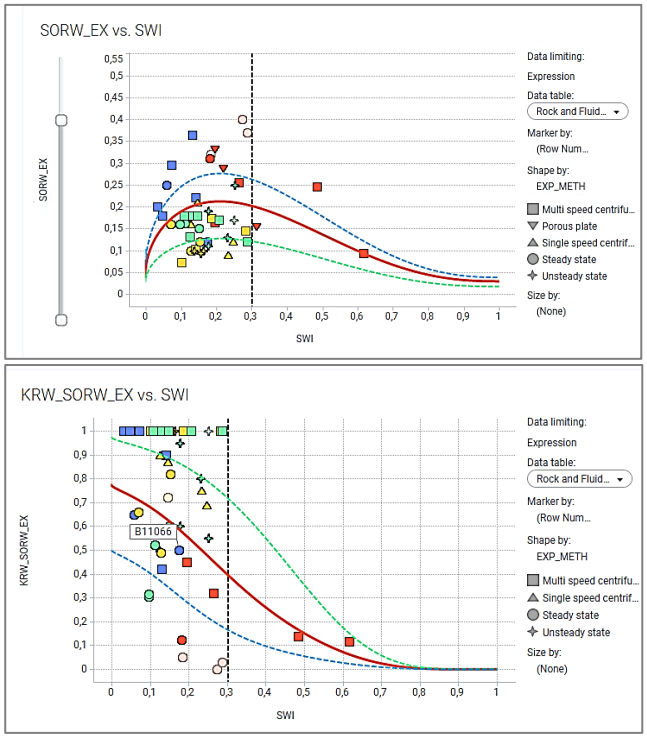

Fig. 12. Experimental data (in red) versus best analogue data. Top) endpoint residual oil saturation, S_{orw} vs S_{wi}, bottom) endpoint water relative permeability, K_{rw} vs S_{wi}.

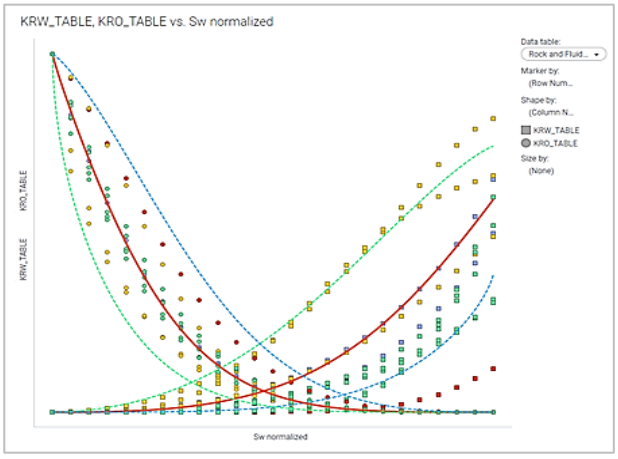

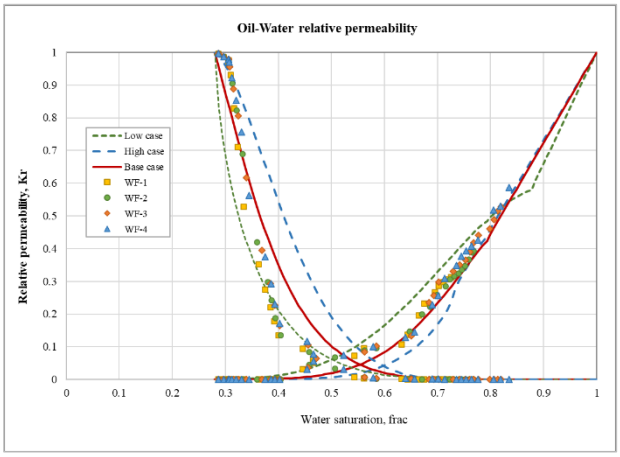

Fig. 13. Top) Field relative permeability model versus experimental data on top. Bottom) Relative permeability model tuned to digital core data at a specific S_{wir} value.

6. Conclusion

This work presents three distinct approaches for determining relative permeability curves. Among the four steady-state experiments conducted, the best one is discussed in this paper, and all curves exhibit high S_{or} and low K_{rw}. However, the wettability of the core plugs, characterized as neutral- to weakly water-wet, fails to explain the observed curvature in the relative permeability curves.

To address this issue, the wettability of the core samples was tested using both mild and harsh cleaning methods. Harsh cleaning modified the samples from oil-wet to weakly water-wet, and it was employed in the new SCAL study. Subsequently, the cleaned cores were aged with crude oil under reservoir conditions, and their wettability was measured using NMR and the standard Amott-USBM indexes. The core plugs exhibited a weak oil-wet behaviour, and there was good agreement between the two methods, suggesting that NMR could serve as a faster and more cost-effective alternative to the Amott test. Endpoint properties were determined through porous plate and multi-speed centrifuge tests, revealing lower S_{or} and higher K_{rw} compared to the steady-state water/oil flooding experiments.

In the second approach, digital rock technology was utilized, although constructing a digital rock model for a laminated core with moderately low porosity and permeability posed challenges. Nevertheless, the petrophysical properties derived from the voxelized binary images showed good agreement with core analysis data. The wettability was defined by adjusting the range of water-advancing contact angles to match the Amott-Harvey Index obtained from the experiments in Section 3.3. The resulting imbibition K_{rw} and K_{ro} curves represented the capillary-dominated (quasi-static) regime. Notably, despite similar porosity and permeability, SP_1 exhibited a larger Sor and smaller K_{rw} (S_{or}) due to its high aspect ratio of large pore bodies to calcite-cement constricted throats.

The third approach involved a methodology that combined existing experimental data with high-quality analogue data sourced from a corporate rock and fluid database. Endpoint functions for saturation and relative permeability, along with LET parameters, were fine-tuned based on a known wettability. The resulting relative permeability curves demonstrated reasonable agreement with experimental and digital rock analysis data.

In conclusion, this study underscores the dependency of flow properties, including wettability, relative permeability, and capillary pressure, on Company best practices and laboratory protocols. Relying solely on a single set of experiments, such as steady-state relative permeability tests, may prove inadequate in capturing the complete range of flow properties. Conducting multiple steady-state experiments can be costly and time-consuming. Alternative methods for wettability determination, such as NMR, along with the collection of comprehensive endpoint data through centrifuge or porous plate experiments, as well as the utilization of digital rock technology, hold promise in providing sufficient data to construct an analytical model for relative permeability.

7. Acknowledgement

The authors would like to thank Norce, SINTEF, PanTerra Geoconsultants and Stratum Reservoir Laboratories for performing the experiments and providing excellent advice. This study is part of a SCAL project for an oil field on the Norwegian Continental Shelf. Therefore, the authors would like to thank AkerBP and our partners, Wintershall Dea Norge and OMV Norge, for funding this project and for allowing to publish these data.

8. References

[1] E. Petersen, A. Larsen, L. Craig, E. Øian, T. Schøyen and E. Zakariassen, "'Rock and Fluid Data: An Integrated Effort on Improving Subsurface Analysis and Modelling Workflows," in *SPE-209538*, Bergen, 2022.

[2] F. Lomeland, "Overview of the LET family of versatile correlation for flow functions," Trondheim, 2018.

[3] C. McPhee, J. Reed and I. Zubizarreta, "Core analysis: a best practice guide," Elsvier, 2015, pp. 322-345.

[4] E. Amott, "Observations Relating to the Wettability of Porous Rock," vol. 216, pp. 156-162, 1956.

[5] W. Looyestijn and J. Hofman, "Quantitative Wettability Index Determination by Nuclear Magnetic Resonance," in *SPEREE*, 2005.

[6] E. Ebeltoft, F. Lomeland, A. Brautaset and A. Haugen, "Parameter based SCAL-Analysing relative permeability for full field application," in *SCA2014-080*, Avignon-France, 2014.